Investigating the Extent of the Impact of Turbulence upon Wind Velocity Profiles

Jack Carlin
Blackett Laboratory
Imperial College London, SW7 2AZ
March 2, 2020

***Abstract*—This report documents the extent of the impact of turbulence on wind velocity profiles. To set about describing the change in wind velocity with altitude, digital thermo-anemometers were used over a small range of heights to record the distribution of wind velocity and temperature with height. This process was repeated over two different surfaces to investigate whether surface conditions strongly affect the profiles. Subsequently, through using auto-correlation analysis we were able to fit the log wind profile model to our data and parameterise the wind flow with two key parameters; the von Karman constant, k, and the surface roughness length, z_0. The derived value of k was 1.94±0.39 over both surfaces, whilst the roughness length of water was found to be 0.7±2.7 mm and the same for grass was 18±11 mm. Despite the numerical uncertainties appearing as strongly limiting, this report sought to find the sources of the error and possible adjustments going forward.**

I. Introduction

THE aim of this experiment was to study wind velocity profiles at varying altitudes, and from that try to draw an inference on the extent of the impact of fluid turbulence on those velocities. The change in wind velocity with height is the *wind gradient* and we were able to build approximations by using mounted digital anemometers at different heights. This data was collected over different days and over different surfaces, in addition to coinciding with Storm Dennis in the United Kingdom [1]. The collected data was processed and analysed with an auto-correlation technique in order to estimate the scale of the wind eddies.

Understanding the wind gradient in the atmospheric surface layer is an important field of study as it allows us to gain a better understanding of the atmospheric circulation at low altitudes, where it most affects society. Geophysical fluid turbulence has recently grown in its area of study from trying to simulate it more accurately [2], to seeing its direct impacts on booming renewable energy markets like wind energy [3] and even solar energy [4]. Thus, by using wind profile analysis techniques as a starting point, simulations can be built up and tested against empirically drawn conclusions.

II. Theoretical Background

The atmospheric boundary layer is the lowest layer of the atmosphere, with the lower limit at 500m [5], which directly interacts with the planetary surface. Here the wind currents are close enough to surface where the geostrophic approximation no longer holds, and thus the wind direction is not necessarily parallel to lower atmosphere isobars. Instead the wind is affected by atmospheric drag causing a wind shear effect, with wind speed decreasing to zero at the surface according to the no-slip condition. Subsequently, the impact of wind turbulence is more pronounced, and is heavily dependent on the physical nature of the underlying surface, something which will be more further investigated throughout this report.

By using the Reynold's Decomposition [6], we can model the wind by thinking of a sum of two velocity terms; the expectation wind velocity, $\bar{u}$, is the general average of the wind velocity within a time constraint, whilst at each time unit there is turbulence in the form of an instantaneous perturbation, u', where $\langle u' \rangle = 0$. As a result, the wind velocity as a function of the height and time can be described as,

$$u(z,t) = \bar{u}(z) + u'(z,t), \tag{1}$$

where $u(z,t)$ is the resultant wind speed. With a notable positive wind gradient the wind shear will exert a momentum flux downwards onto the surface, known as a shearing stress, η. Due to the wind velocity that applies this stress is in the horizontal direction it is analogous to friction and can thus be described through Newton's Law of Friction as,

$$\eta = \rho K_m(z) \frac{\partial u}{\partial z}, \tag{2}$$

where ρ is the mass density of the passing air, and $K_m(z)$ is the kinematic eddy viscosity which for the purpose of this report is only a function of altitude and is a measure of the momentum transmissivity of the eddy, despite having a noticeable dependence on local Reynold's Number [7].

From Eq. 1, it can be shown that the average wind velocity can be rewritten with a logarithmic relationship to height in order to get a more complete relationship,

$$\bar{u}(z) = \frac{u^*}{k} \ln\Big(\frac{z}{z_0}\Big), \tag{3}$$

where k is the von Karman constant, z_0 is the roughness length, and u^* is the shear velocity. As long as horizontal turbulence, u', and the vertical turbulence, w', are of similar magnitudes then the shear velocity can be approximately described as,

$$u^* = \sqrt{u'w'}. \tag{4}$$

Furthermore, the surface roughness length, z_0, manifests itself as a constant of integration and, whilst not actually a physical length, it represents the height at which the horizontal wind velocity theoretically becomes zero.

The relationship described in Eq. 3 depends on the approximation that the atmosphere is neutrally buoyant, and thus in order to make sure that the data can be analysed using the aforementioned equations, we must consider the Richardson

Number. The Richardson Number, Ri, paramaterises the dominance of either buoyancy-driven turbulence or shear-driven turbulence. It does this by creating a ratio of their effects which is described as,

$$Ri = \frac{\text{buoyancy effect}}{\text{shear effect}} = \frac{g}{T} \cdot \frac{\frac{dT}{dz}}{\left(\frac{du}{dz}\right)^2}, \tag{5}$$

where g is the gravitational acceleration and T is the local temperature, whilst the derivative of temperature with respect to height is known as the adiabatic lapse rate. Therefore, if the Richardson number is notably smaller than unity [8], we can say that the local atmosphere is approximately neutral and thus the previous equations are valid.

III. Methodology

To obtain the data required to study the effect of turbulence in wind velocity profiles, we used digital anemometers with an in-built thermometer mounted onto a three metre high tripod. Six anemometers were used in total, three pairs of anemometers placed one metre apart; at each height level one device would record the vertical wind velocity element, whilst the other for the horizontal wind velocity. The data was taken in Hyde Park in London, England, with majority of the data points obtained over the course of the 17$^{\text{th}}$ of February, 2020. At that time the United Kingdom was affected by Storm Dennis, an extra-tropical windstorm, which resulted in a maximum gust speed of 27 $\mathrm{m\,s^{-1}}$ in London [1].

In order to take the highest quality wind velocity recordings it is important to have very few vertical obstacles so that the only contributor to the turbulence is the surface structure. However, with London being a densely populated city, it proved difficult to find a suitable location devoid of obstacles. Nevertheless, an open enough area was settled on that ensured that the majority of the turbulence arose due to the underlying surface.

In addition to the field work, the anemometers were tested in the lab to investigate how their inherent properties may affect the dataset. It was concluded that this could come about in two predominant ways. Firstly, each anemometer had its own reading offset which meant that they were tested with a constant wind velocity coming from a electric propeller-style fan. Furthermore, these offsets were tested at different wind velocities so that we could investigate if they vary with higher wind speeds given the strong gusts that were experienced during collection. The other key test was the response time of the sensors and if that also changed with wind speed; an important to check to see how much data is missed.

A. Anemometer Calibration

A brace was set up to point the anemometers perpendicular to the face of the fan so that all the sensors were at the exact same position relative to the fan. The fan had 4 different speed settings; at each setting, ten readings were taken in order to find an average reading and its variance. This process was repeated for all six anemometers. Once they were all tested and their average reading was found, a *true* reading was found, which was the average of averages. Using the true reading as a reference, the deviation of each anemometer could be defined and subsequently a scaling factor was found for each sensor.

As shown in Fig. 1, the anemometers consistently displayed a linear trend of the statistical error with an increasing reading of wind velocity. This consistency meant that the scaling factors could be applied to the corresponding anemometers total set of readings by using a weighted average of each velocity level. Despite Fig. 1 only showing the horizontal velocity

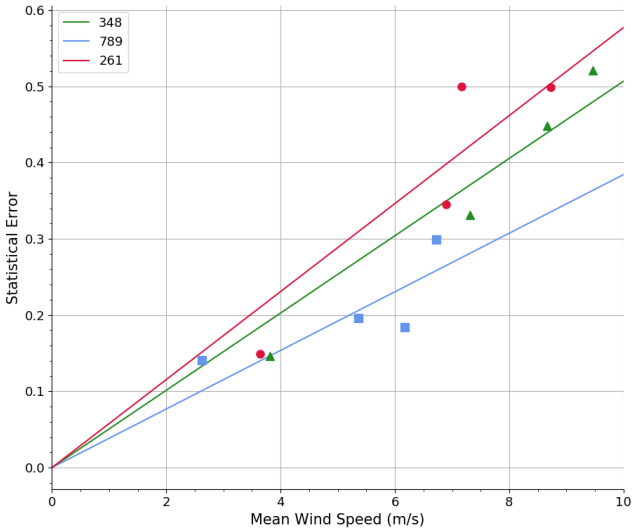

Fig. 1. A plot of statistical error (standard deviation) against the mean wind speed of ten readings taken on three different anemometers (Models 348, 789, and 261). These three anemometers were used for the horizontal wind readings. The calibration data is plotted as points with a linear fit on them. The gradients of these lines are 0.057, 0.058, and 0.052 for the models respectively.

sensors, across all six anemometers the average uncertainty percentage of the linear fits was 0.596%. It is worth noting that the uncertainty comes from the variance of the linear fit, which is realised by a Levenberg–Marquardt least-squares algorithm. This algorithm uses the points to find the optimal linear trend however there may be non-quantitative uncertainty on the points which was not taken into account. Nevertheless, to a reasonable extent this linear relationship was consistent and thus deemed suitable for the investigation.

B. Response Time

The response time was ascertained by recording the readings of incident wind velocity from an approximately static environment to an abrupt increase in wind velocity using a propeller fan. The wind velocity was then progressed across three different settings to see if the response time was a function of incident velocity. The findings of this investigation can be seen in Fig. 2. The average response time over all six anemometers was 6 ± 1 seconds, whilst the uncertainty in that value comes from the anemometer only producing readings every two seconds.

The response time stayed consistent across different velocities and thus we could say that, for the investigation, the response time is independent of incident wind velocity. Initially this presented itself as a limitation of the experiment

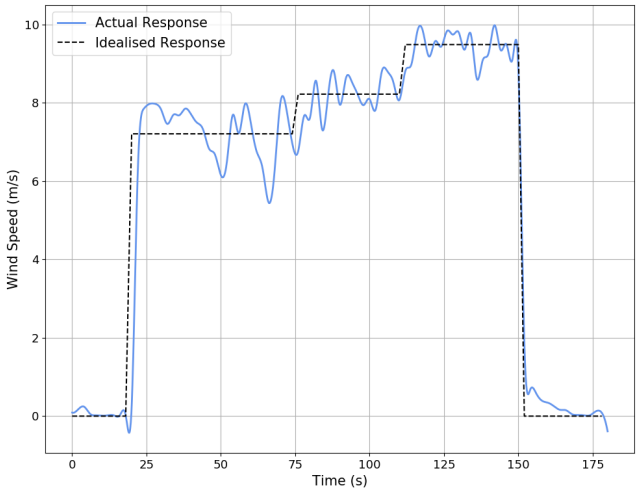

Fig. 2. A plot of horizontal velocity recorded against the time elapsed used to make an estimation of the anemometers response time. The idealised response is overlaid and shows that there is a consistent lag between each velocity setting.

because much of the wind variation measurements will be lost in the time in between. Theoretically the variation will solely come from the wind turbulence, which is the key part of the investigation and so losing those data points would affect the results. However, due to the set up of the apparatus in the strong winds, there was a oscillation of the brace parallel to the horizontal axis, which would have altered the results due to the relative motion of the anemometer and the wind. Subsequently, the response time would ensure that the majority of this effect was phased out as the rattling period was less than that of the response time.

IV. Results and Discussion

Using the method outlined above to scale the recorded data, the wind speed profile was collated and is presented in Fig. 3, over surfaces of grassland and water. Both plots in Fig. 3 show the $\bar{u}(z)$ term as opposed to the complete wind velocity term in order to show the trending of the wind speed on average. As expected the wind velocity seems to have no predictable trend solely from the data; a meteorological prediction model would have to be used to predict wind speed variation over the course of a day. Additionally, the wind gradient came out as expected in the sense that it the velocity uniformly increases with height notwithstanding the error bar overlap.

As aforementioned, in order to extract the average wind velocity from the highly variable data set, the use of a moving average was employed. This allowed the data set to be decomposed into an oscillatory and a slowly varying component. The moving average was executed by consecutively averaging small subsets of the time series at a period which was defined by auto-correlation analysis. The auto-correlation was necessary to ascertain the time-scale of the effect of a singular eddy. By recording the changing standard deviation of the time series, auto-correlation can reveal at what points in the time series a subset of variations is no longer correlated to the previous subset. In the case of this investigation, that is manifested within the point at which the turbulence is caused by a new eddy structure.

The results of the auto-correlation analysis can be seen in Fig. 4. In order to acquire a value for the period used in the moving average, an exponential decline was fitted to the relationship using least-squares, and the largest decay time of all the anemometers was used as the period.

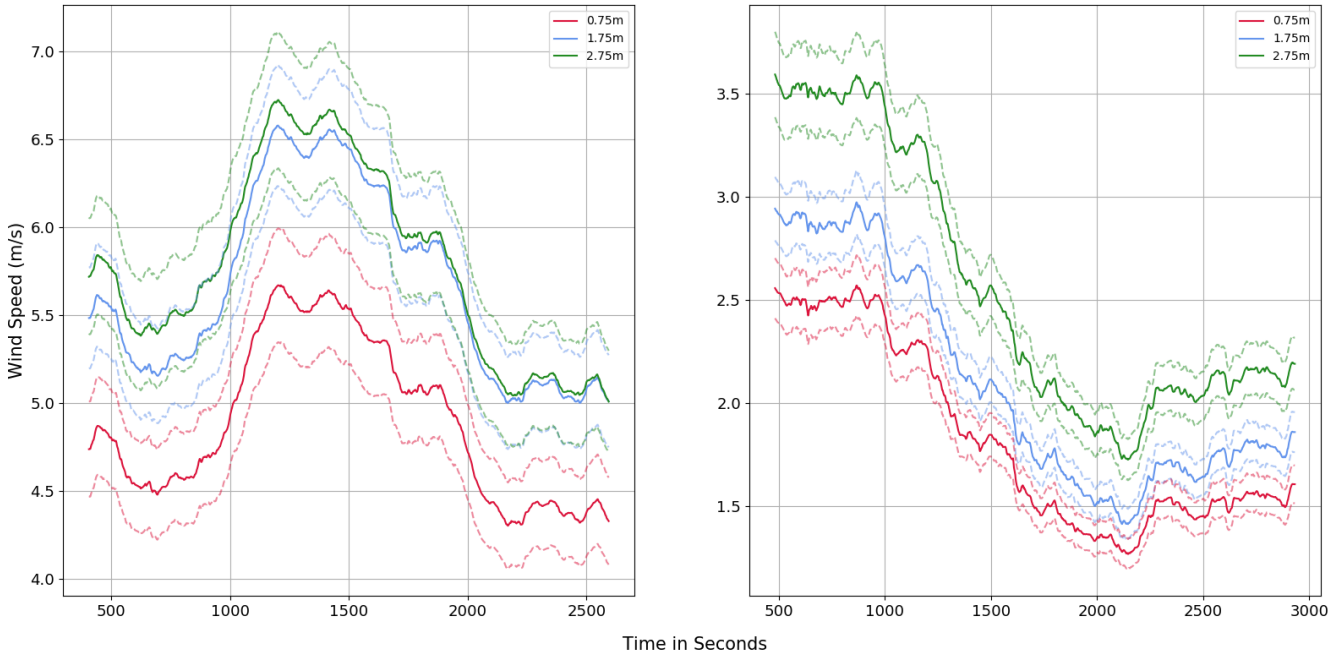

Fig. 3. The plot shows the wind velocity profile against the elapsed time over water (left) and over grass (right). Dashed lines denote $\pm\sigma$ for their colour.

In Section II, it was mentioned that the logarithmic relationship used to model wind speed with height hinged on the Richardson number, Ri, which attempted to describe the dominance of buoyancy over the shear effect. Essentially contrasting free geostrophic circulation, against a turbulent atmosphere that is dominated by wind shearing. Consequently, before moving forward onto the analysis of this proposed logarithmic relationship, it was required that the Richardson number that the data produced, using Eq. 5, was sufficiently small to warrant the use of such analysis. The distribution

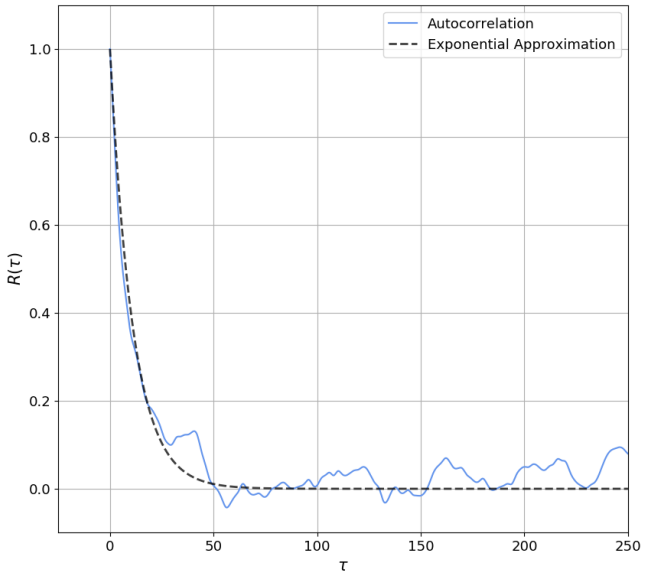

Fig. 4. A plot of the auto-correlation, $R(\tau)$, against the time lag, τ. This is overlaid with a decaying exponential fit that was used to approximate the integral of $R(\tau)$ with respect to τ, which describes the maximum period.

of Ri from the data can be seen in Fig. 5, over surfaces of water and grass. Both histograms show that the data approximately meets the criteria for the logarithmic analysis. More specifically, a larger percentage of the wind velocities passing over water satisfy a strict criterion of -0.01 $< Ri <$ 0.01. This result is likely due to the higher wind speeds of the dataset over water; the higher velocities over the water surface will lead to a larger friction velocity, u^*, and subsequently this means that the effect of wind shear is larger.

Consequently, the data could be processed into the form described in Eq. 3, however an approximation of u^* had to be made in order to solve for the von Karman constant. This approximation is outlined in Eq. 4 and only holds when u' and w' are of similar magnitudes. The results of this can be seen in Table I, which shows the root-mean-square residual turbulent components derived from the $\bar{u}(z)$ profile seen in Fig. 3, input into the Reynolds Decomposition outlined in Eq. 1; at all heights the vertical and horizontal turbulent components were on the same order of magnitude and thus the table is also able to show the resultant friction velocity.

Once the mean friction velocities were found, the data could be investigated to see if it fit the form shown in Eq. 3, and from that find values for the von Karman constant, k, and the roughness length, z_0. The logarithmic fit onto the

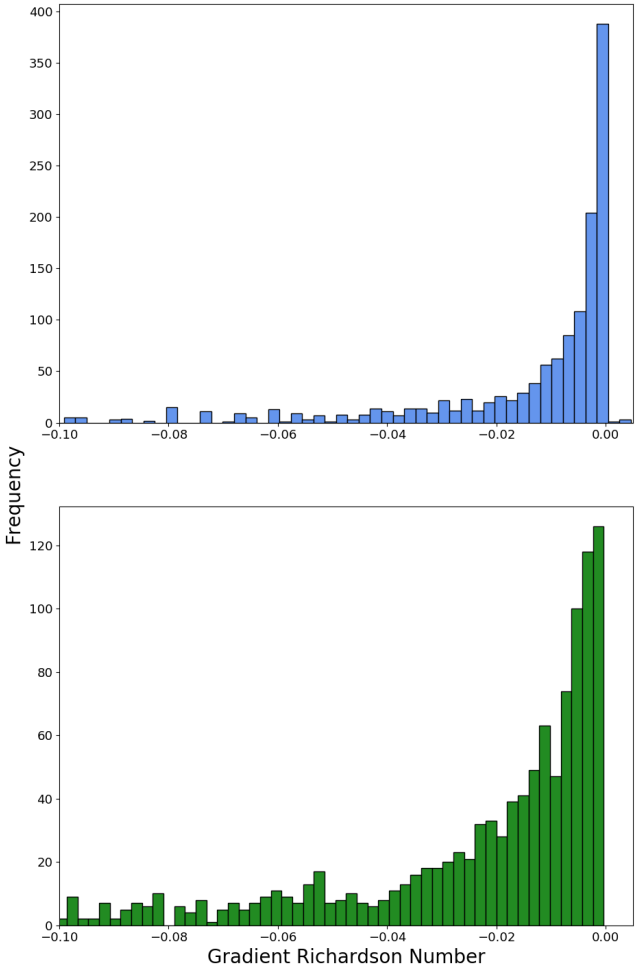

Fig. 5. The histogram shows the distribution of recorded gradient Richardson Numbers, Ri, from the data over water (top) and over grass (bottom). Over water, 65% of the recorded Richardson numbers meet the criterion $|Ri|< 0.01$, whereas for the wind flow over grass, only 29% meet that same condition.

z (m)	u'_{rms} ($\mathrm{m\,s^{-1}}$)	w'_{rms} ($\mathrm{m\,s^{-1}}$)	u^* ($\mathrm{m\,s^{-1}}$)
Grass			
0.75	1.94	0.52	1.01
1.75	2.28	0.74	1.30
2.75	2.26	0.87	1.40
Mean u^*			1.24
Water			
0.75	1.77	0.87	1.24
1.75	2.01	1.25	1.59
2.75	1.90	1.12	1.46
Mean u^*			1.43

TABLE I

wind velocity data over water and grass is displayed in Fig. 6. Furthermore, Fig. 6 only represents data over one period of the running mean, which in turn is iteratively applied over the whole dataset in order to extract a value of k and z_0 representing the whole varying mean, $\bar{u}(z)$. In particular for Fig. 6, the von Karman constant for the specific data subset over water came out as 1.70±0.77, whilst the roughness length of the water is shown as 0.9±2.9 mm, overall with a chi-squared confidence of 59%. On the other hand, the wind velocity data subset over grass produced a von Karman constant of 2.27±0.69 and a roughness length of 15±19 mm,

with a lower confidence of 20%. The error for a particular subset is significantly high however as this process is iterated over the whole dataset the statistical error will decrease given the larger quantity of considered data points. As a result the final parameters for the two surfaces were found and are shown with their uncertainties in Table II.

Parameter	Value	Uncertainty
Water		
k	1.74	0.55
z_0/mm	0.7	2.7
Grass		
k	2.14	0.37
z_0/mm	18	11

TABLE II

The von Karman constant is theoretically independent of surface condition [9] as it is only a description of proportionality between altitude and mixing length for eddies. As a result, it was deemed appropriate to average the constants for both the grass and water surface in order to obtain a final approximation of k for the investigation, which comes out as **1.94±0.39**.

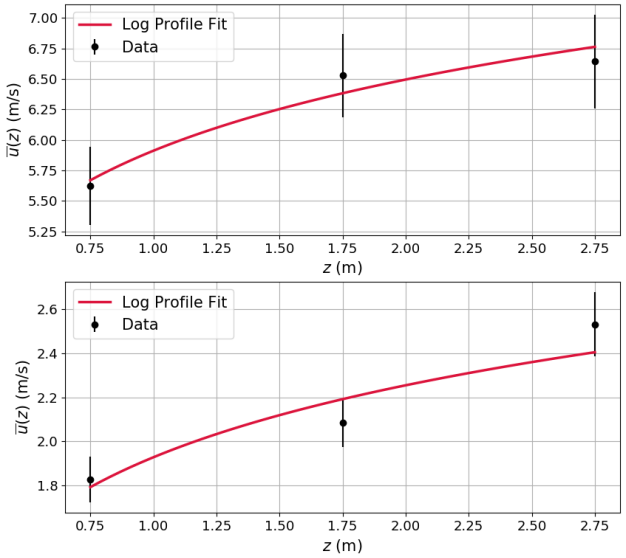

Fig. 6. The plot shows the local average wind speed, $\bar{u}(z)$ at each recording height for the data of wind flow over water (above) and over grass (below). The log wind profile fit is overlaid on the data and accounts for the error bars. Notably the datapoints exhibit a large uncertainty due to this plot in particular only showing the relationship for a small subset of $\bar{u}(z)$ instead of the whole profile.

This values of roughness length, z_0, for both surfaces of water and grass stayed consistent with other studies. One such study carried out in 1993 concluded that short grass exhibited a roughness length of 0.5 to 2 cm, whilst open water had a range of 0.1 to 1 mm [10]. Both roughness lengths concluded by this investigation fall comfortably within those ranges. On the other hand, the empirically accepted value for the von Karman constant, k, is consistently found to be 0.4. Recent studies find that the constant clusters around ranges of 0.37 - 0.39 and 0.42 - 0.43 [11].

Given that the values for the roughness length seem to be logical and consistent with outside literature, it is likely that the recorded form of the wind velocity profile is accurate enough to produce a high confidence in z_0, however the individually recorded velocities may be inaccurate causing a drastically different k. One possible source of this inaccuracy comes from the variation in the incident angle of the mass flux onto the anemometer. This could result in an overestimation of the friction velocity, u^*, or an underestimation of the local mean wind speed, $\bar{u}$. A high variation speed of the angle will appear as turbulence in the dataset and thus contributing more to the shear effect, whereas an underestimation in the average wind speed may come about from the incident wind no longer being perpendicular and thus only a lesser component of that wind vector is recorded instead. A manifestation of this effect may also be displayed in Table I, where u'_{rms}, despite being on the same order of magnitude, is over three times that of w'_{rms} on average. The expectation was that these would be very similar however the horizontal component of turbulence is notably larger, which is plausibly due to this angular variation.

V. Conclusion

To conclude, the aim of the experiment was to build a wind velocity profile across a range of heights to see if recorded data would fit the theoretical framework. This aim was only marginally achieved because, whilst the data did fit the proposed logarithmic relationship, the parameterisation that came with it was only half successful. The two parameters which were used to describe the model were the roughness length of the surface, z_0, and the von Karman constant, k. The roughness length was well approximated and fit the general trend with outside literature, however the von Karman constant was not successfully approximated and showed large deviation from the empirically accepted value. We were able to identify a possible source of inaccuracy, coming from the data taking process.

Moving forward, two key changes to the experiment would possibly show a better degree of success. Firstly, if data was taken in a more open environment then the apparent change in wind direction would be lessened as there would be a more uniform local mass flux. In addition, a better sampling of heights, going further than just 2.75 m, would provide a more accurate wind velocity profile and would allow for derivatives of wind velocity with respect to height to be evaluated at more than one point when using a central differencing scheme.

References

[1] M. Kendon, *Storm Dennis Report*, UK Met Office National Climate Information Centre, Feb. 2020.

[2] A. Ricci, I. Kalkman, B. Blocken, M. Burlando, and M. Repetto, "Impact of turbulence models and roughness height in 3d steady rans simulations of wind flow in an urban environment," *Building and Environment*, vol. 171, p. 106 617, 2020.

[3] R. Lanzafame, S. Mauro, and M. Messina, "Wind turbine cfd modeling using a correlation-based transitional model," *Renewable Energy*, vol. 52, pp. 31–39, 2013.

[4] F. Fouladi, P. Henshaw, D. S.-K. Ting, and S. Ray, "Wind turbulence impact on solar energy harvesting," *Heat Transfer Engineering*, vol. 41, no. 5, pp. 407–417, 2020.

[5] J. E. Cermak, "Laboratory simulation of the atmospheric boundary layer," *Aiaa Journal*, vol. 9, no. 9, pp. 1746–1754, 1971.

[6] R. J. Adrian, C. D. Meinhart, and C. D. Tomkins, "Vortex organization in the outer region of the turbulent boundary layer," *Journal of fluid Mechanics*, vol. 422, pp. 1–54, 2000.

[7] G. Maise and H. McDonald, "Mixing length and kinematic eddy viscosity in a compressible boundary layer.," *AIAA Journal*, vol. 6, no. 1, pp. 73–80, 1968.

[8] J. S. Rodrigo, E. Cantero, B. Garcia, F. Borbón, U. Irigoyen, S. Lozano, P. Fernande, and R. Chávez, "Atmospheric stability assessment for the characterization of offshore wind conditions," in *Journal of Physics: Conference Series*, IOP Publishing, vol. 625, 2015, p. 012 044.

[9] U. Högström, "Review of some basic characteristics of the atmospheric surface layer," *Boundary-Layer Meteorology*, vol. 78, no. 3-4, pp. 215–246, 1996.

[10] F. V. Hansen, "Surface roughness lengths," ARMY RESEARCH LAB WHITE SANDS MISSILE RANGE NM, Tech. Rep., 1993.

[11] E. L. Andreas, K. J. Claffey, R. E. Jordan, C. W. Fairall, P. S. Guest, P. O. G. Persson, and A. A. Grachev, "Evaluations of the von kármán constant in the atmospheric surface layer," *Journal of Fluid Mechanics*, vol. 559, pp. 117–149, 2006.